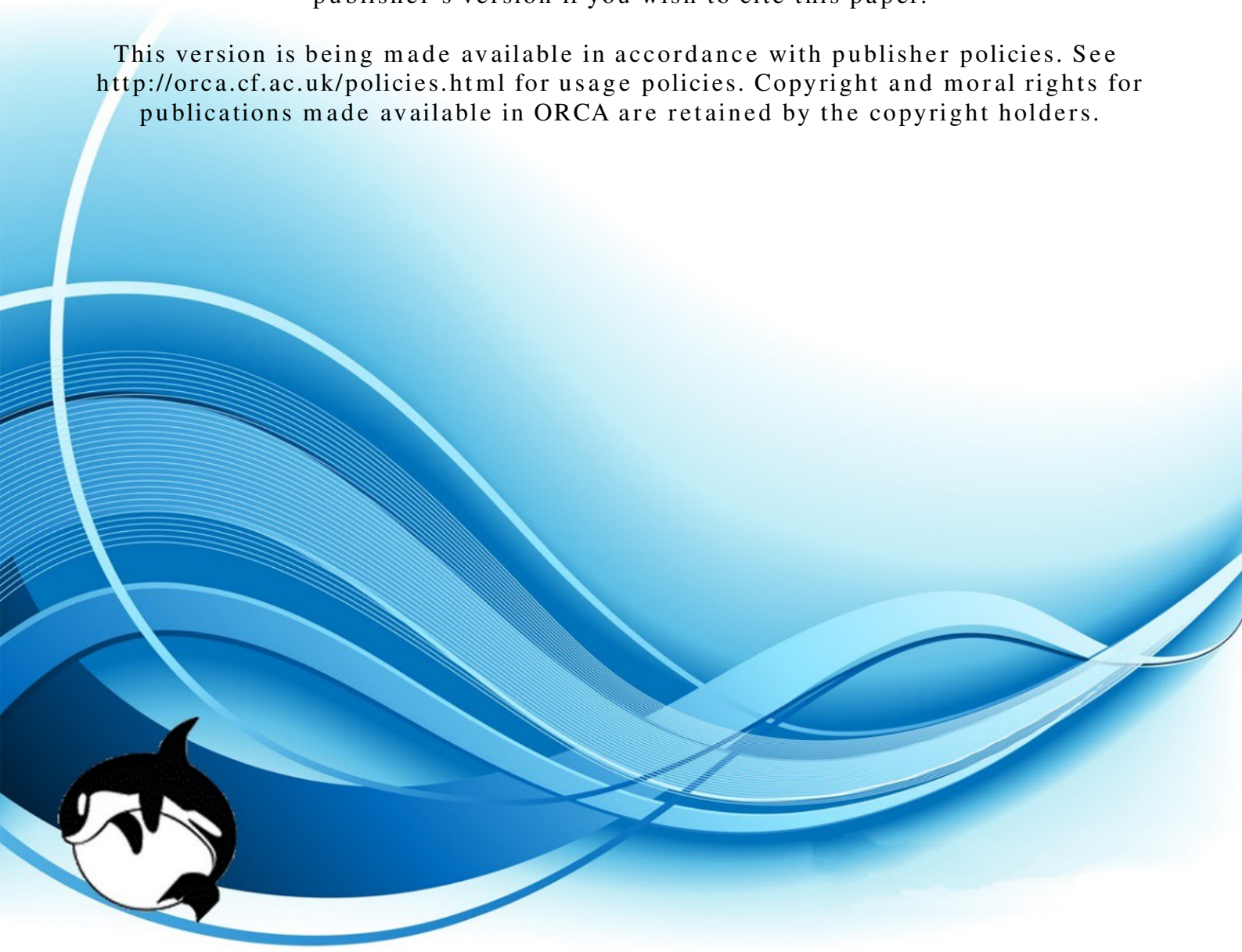

Continuous-wave lasing from InP/InGaAs nano-ridges at telecommunication wavelengths

Yu Han[1], Qiang Li[1], Si Zhu[1], Kar Wei Ng[2], and Kei May Lau[1, a)]

[1]Department of Electronic and Computer Engineering, Hong Kong University of Science and Technology, Clear Water Bay, Kowloon, Hong Kong, China

[2] Institute of Applied Physics and Materials Engineering, University of Macau, Avenida da Universidade, Macau, China

(Postal codes are not available in both Hong Kong and Macau)

[a)] Tel: (852)23587049, Fax: (852) 23581485, Email: eekmlau@ust.hk

Abstract

We report continuous-wave lasing from InP/InGaAs nano-ridges grown on patterned (001) Si substrate by aspect ratio trapping. Multi-InGaAs ridge quantum wells inside InP nano-ridges are designed as active gain materials for emission in the 1500 nm band. The good crystalline quality and optical property of the InGaAs QWs are attested by transmission electron microscopy and micro-photoluminescence measurements. After transfer of the InP/InGaAs nano-ridges onto a SiO_2/Si substrate, amplified Fabry-Perot resonant modes at room temperature and multi-mode lasing behavior in the 1400 nm band under continuous-wave optical pumping at 4.5 K are observed. This result thus marks an important step towards integrating InP/InGaAs nano-lasers directly grown on microelectronic standard (001) Si substrates.

This manuscript was accepted by Appl. Phys. Lett. Click here to see the version of record.

Semiconductor nanowires are emerging as ideal building blocks for ultra-compact optoelectronic devices with low-energy dissipation.[1] As a result of axially guided optical modes and feedback provided by end-facets, lasing behaviors have been observed in various II-VI and III-V compound semiconductor nano-structures.[2-16] In particular, indium phosphide (InP) and indium gallium arsenide (InGaAs) nano-lasers, emitting at silicon(Si)-transparent wavelengths, show great promise to fill a key missing on-chip component in Si photonics based optical interconnects.[17-21] However, most of the previously demonstrated InP/InGaAs nano-lasers operate under pulsed-conditions.[22-24] Continuous-wave (CW) lasing at telecom-wavelengths has only been achieved in InP/InGaAs nano-pillars grown on (111) Si substrates[25] and InAsP/InP nanowires (inside Si photonic crystal cavity) grown on (111)B InP substrates, with lasing wavelengths situated at the 1200 and 1300 nm bands.[26] Extending the lasing wavelengths to the 1400 nm and 1500 nm bands is desirable for high density inter/intra-chip data transmission. In this letter, we utilized InP/InGaAs nano-ridges grown on (001) Si substrate to demonstrate CW lasing behavior at the 1400 nm band.

Compared with other hetero-epitaxial growth techniques, selective area growth combined with the aspect ratio trapping (ART) method provides a viable route to form well-aligned, millimeter-long horizontal in-plane nanowires on CMOS-standard (001) Si substrate.[27-34] Previously, we have leveraged this approach to grow InP nano-ridges with embedded InGaAs quantum wells (QWs) and quasi-quantum wires (QWRs) with strong photolumiescence.[35-36] Here, we observe CW lasing at the telecommunication band from high quality multi-InGaAs ridge QWs inside the InP nano-ridges directly grown on nano-patterned silicon. To explore the potential of the InP/InGaAs nano-ridges as nano-scale light sources, we separated the InP/InGaAs nano-ridges from the initial patterned Si substrate and transferred them onto a SiO_2/Si substrate for optical characterization.

This manuscript was accepted by Appl. Phys. Lett. Click here to see the version of record.

We observed CW lasing at 4.5 K under optical excitation, and strong optical mode modulation at room temperature.

The InP/InGaAs nano-ridges used in this experiment were grown on (001) Si substrates using a metal-organic chemical vapor deposition (MOCVD) system with a horizontal reactor (AIXTRON 200/4). [110] direction oriented SiO_2 stripe patterns with a line pitch of 1 μm and a trench opening width of 450 nm were used to define the growth regions. Detailed sample preparation and growth procedure have been reported elsewhere.[35-36] Fig.1 (a) presents the top-view scanning electron microscope (SEM) image of the as-grown sample, showing uniform morphology across a large area. The 70° tilted-view SEM image in Fig. 1 (b) reveals symmetrical {111} faceting. A zoomed-in SEM image in Fig. 1 (c) highlights the multi-QW active region. Notably, to enhance contrast, the InGaAs layers were selectively etched in a H_2PO_4:H_2O_2:H_2O (3:1:50) solution. Five uniform InGaAs ridge QWs and the GaAs nucleation buffer are clearly identified.

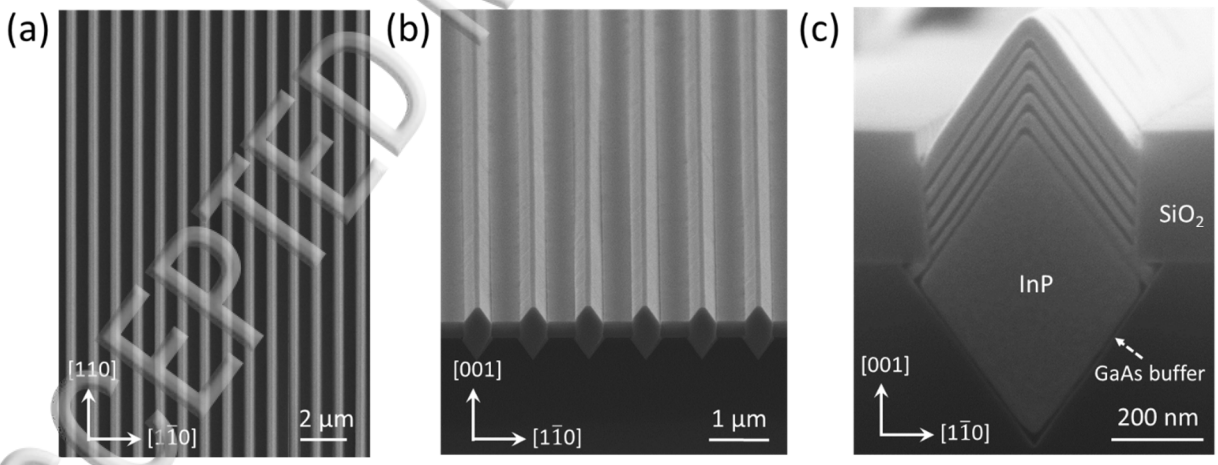

Figure 1.

Transmission electron microscope (TEM) has been used to characterize the structural properties of the InGaAs ridge QWs. We prepared the TEM specimens by mechanical polishing and subsequent ion beam milling, and examined the samples in a JEOL2010 field-emission

This manuscript was accepted by Appl. Phys. Lett. Click here to see the version of record.

microscope under multiple-beam conditions. The cross sectional TEM image in Fig. 2(a) indicates a large strain field in the vicinity of the III-V/Si hetero-interface. With most of threading dislocations confined at the bottom of the V-shaped pocket, a few stacking faults still propagate into the InP main layer above the V-groove (see Fig. 2(b)). Fig. 2(c) displays the zoomed-in TEM image of the tip region of the InGaAs ridge QWs. The thicker regions at the tip area results from the growth preference at the transitional facets.[37] Fig. 2(d) presents the five InGaAs ridge QWs on one side of the InP nano-ridge. The 7 nm thick InGaAs ridge QWs and 28 nm thick InP spacers exhibit a sharp interface and a uniform thickness along the {111} facets. A TEM image recorded along the trench direction is shown in Fig. 2(e). The yellow dotted line marks the boundary between the InP buffer inside and outside the V-grooved pocket. While the bottom part of the InP buffer is quite defective, the upper part, where the InGaAs ridge QWs reside, exhibits good crystalline quality. The zoomed-in TEM image in Fig. 2(f) exemplifies the generation of threading dislocations and stacking faults at the III-V/Si interface. Optical properties of the InGaAs ridge QWs were investigated by micro-photoluminescence (μ-PL) measurements. Fig. 3 displays the normalized PL spectra measured at 4.5 K and 300 K. At 4.5 K, the central emitting wavelength of the ridge QWs lies at 1436 nm with a full-width-at-maximum (FWHM) of 125 nm. At room temperature, the central emitting wavelength shifts to 1490 nm due to band gap shrinkage at higher temperatures. The FWHM also increases to 147 nm from thermal broadening. Assuming a unit internal quantum efficiency (IQE) at 4.5 K, an IQE of 29.7% is extracted at room temperature under a relatively low excitation power density of 320 W/cm^2. To avoid carrier localization at the cross-over region of the {111} facets, we tuned the growth conditions of the InGaAs QWs for a dominant emission, as manifested by the characteristics of single-peaked PL spectra at both 4.5 K and 300 K.

This manuscript was accepted by Appl. Phys. Lett. Click here to see the version of record.

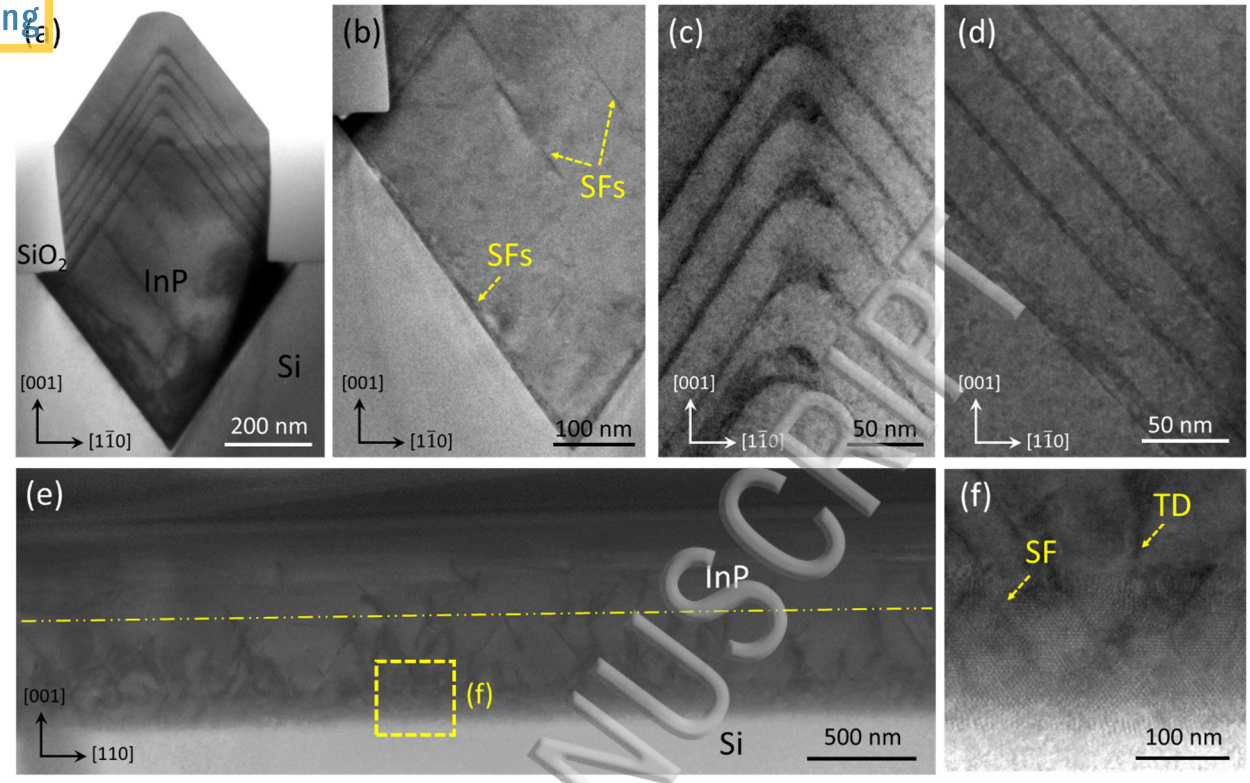

Figure 2.

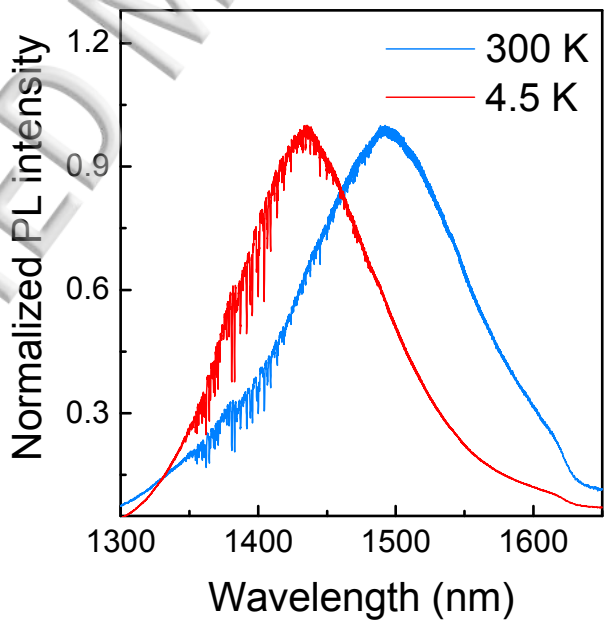

Figure 3.

This manuscript was accepted by Appl. Phys. Lett. Click here to see the version of record.

For nano-lasers directly grown on V-grooved Si, minimizing light leakage into the bulk Si substrate is essential to realize lasing. Improved optical confinement can be achieved by transferring the nano-ridges onto an oxide substrate,[9] etching away the underlying Si,[13,24] or direct hetero-epitaxy on a silicon-on-insulator (SOI) substrate.[38] To exploit the potential of these InP/InGaAs nano-ridges as nano-scale light sources, we adopted the first method to evaluate the quality of the active medium grown on silicon. After removing the SiO_2 spacers by buffered oxide etch (BOE) and undercutting the Si in a KOH solution, the InP/InGaAs nano-ridges were separated from the initial Si substrate in ultrasonic bath and transferred onto a SiO_2/Si substrate (1 μm thick SiO_2). The directions of the transferred InP/InGaAs nano-ridges are completely random. Fig.4 (a) presents a schematic of the transferred InP/InGaAs nano-ridge and the excitation/detection scheme. Fig. 4(b) shows the microscope image of a transferred 32 μm long InP/InGaAs nano-ridge on the SiO_2/Si substrate. The zoomed-in SEM image reveals a smooth and vertical (110) end-facet, which is essential for strong optical feedback. The as-grown convex (111) facet is labeled in yellow and the $(\bar{1}10)$ facet originally contacting with the SiO_2 sidewall is labeled in red (see Fig. 4(b)). The low-temperature GaAs nucleation buffer and the InP main layer are also distinguishable.

We first investigated the optical characteristics of the transferred InP/InGaAs nano-ridges through room temperature μ-PL measurements. Excitation was provided by a CW 1064 nm laser with a shaped rectangular beam (40 μm × 4 μm), and light emission was collected by a thermoelectric-cooled InGaAs detector through the same objective (0.1 nm spectral resolution). During the measurements, the laser spot was aligned to fully cover the InP/InGaAs nano-ridge. Fig. 4 (c) displays the measured PL spectra under different excitation power density. At low pumping power density, the InP/InGaAs nano-ridge exhibits a broad spontaneous emission spectrum with fine Fabry-Perot (FP) resonant peaks. The free-spectral- range (FSR) of the cavity

This manuscript was accepted by Appl. Phys. Lett. Click here to see the version of record.

modes (8.6 nm at 1500 nm band) agrees well with the length (32 μm) of the measured InP/InGaAs nano-ridge. As the pumping power density increases, the overall peak of emission slightly blue-shifted due to state-filling effects at higher excitation levels. More importantly, the FP modes become stronger compared with the background spontaneous emission and the line-width of the FP modes continues to decrease, suggesting the transition from spontaneous emission to amplified spontaneous emission. In fact, as pumping power density increases from 2.90 kW/cm^2 to 6.63 kW/cm^2 and then to 16.8 kW/cm^2, the line-width of the peak at 1468 nm decreases from 3.50 nm to 1.93 nm and then to 1.59 nm.

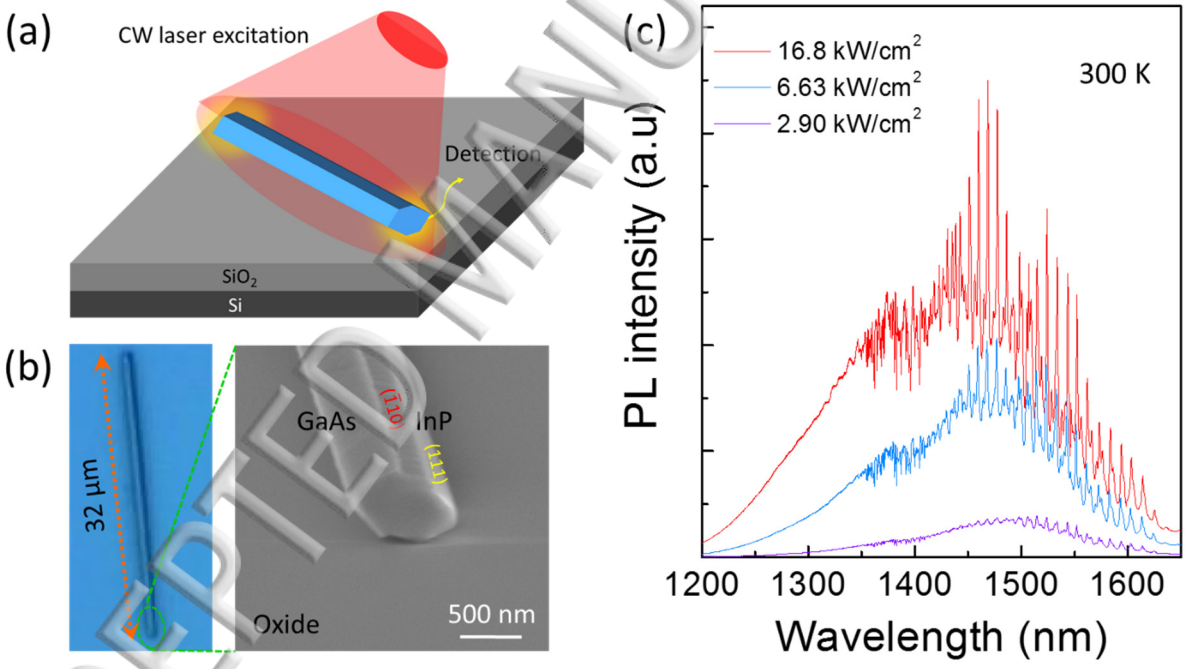

Figure 4.

Multi-mode lasing was observed at 4.5 K, as illustrated by the emission spectra under different pumping levels in Fig. 5(a). At low excitation levels, the InP/InGaAs nano-ridge emits a broad spontaneous spectra with discernable FP resonance peaks from 1400 nm to 1500 nm. As the

excitation level increases, the peaks situated at 1410 nm and 1418 nm intensify and stand out from the background emission, indicating the transition from spontaneous emission to stimulated emission. Fig.5 (b) shows the light-light (L-L) curve and line-width of the peak at 1410 nm as a function of excitation power density. A clear threshold knee is observed in the L-L curve and the threshold is extracted to be around 6.5 kW/cm^2. Lasing behavior is further evidenced by the decrease of the line-width and the subsequent clamping at 0.4 nm as excitation level increases beyond threshold. Fig. 5(c) illustrates the blue-shift of the peak at 1410 nm as the pumping power density increases, which could be attributed to the band-filling effects in the multi-InGaAs QWs. Similar behavior has also been observed in other nano-lasers using multi-QWs as gain medium.[39] Fig. 5 (d) presents the cavity modes at 1410 nm and 1418 nm under a low excitation level. The FSR between the two modes is extracted as 7.7 nm and the line-widths are 0.48 nm and 0.52 nm, respectively. We estimated the quality factor (Q-factor) of the nano-ridge as $Q = \lambda/\Delta\lambda = 2938$. This Q-value is substantially higher than other reported nano-lasers emitting in the near-infrared range. We attributed the high Q-factor of our InP/InGaAs nano-laser to the long length of the cavity and the high quality of the end-fact. The lasing mode was identified to be TE_{01} by simulating the electrical filed distribution inside the ridge waveguide, as it exhibits the best overlap with the active region among all the existing propagation modes (see the inset in Fig. 5(d)). We observed similar lasing behavior from other transferred InP/InGaAs nano-ridges with length around 30 μm and lasing wavelength around 1410 nm.

This manuscript was accepted by Appl. Phys. Lett. Click here to see the version of record.

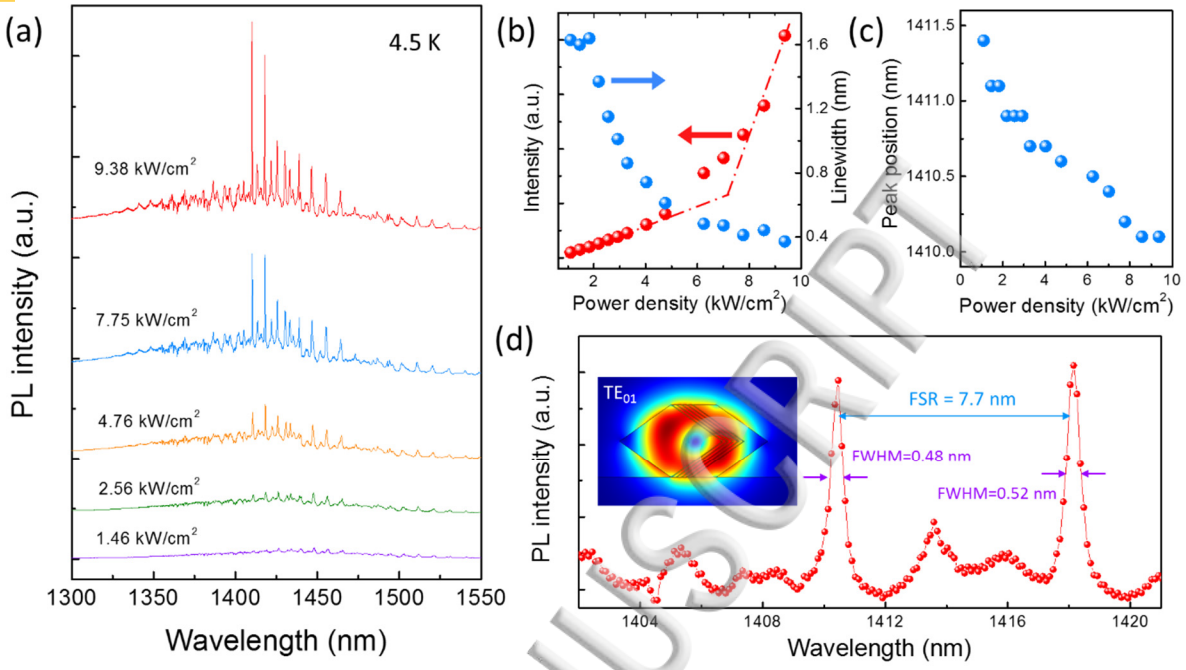

Figure 5

In conclusion, we have demonstrated CW lasing at the 1400 nm band from InP/InGaAs nano-ridges initially grown on an exact (001) Si substrate. Clear lasing threshold can be identified from the L-L curves and line-width narrowing of the emission peak are detected at 4.5 K under optical excitation. Moreover, we observed strong FP mode modulation and amplified spontaneous emission at room temperature. The CW lasing behavior from the transferred InP/InGaAs nano-ridges thus demonstrate the high optical property of the multi-InGaAs ridge QWs inside InP nano-ridge, and show the potential of integrating InP/InGaAs nano-lasers, emitting at telecommunication wavelengths, onto microelectronic standard (001) Si substrates.

Acknowledgements

This work was supported in part by Grants (Nos. 614813 and 16212115) from the Research Grants Council of Hong Kong and in part by the Innovation Technology Fund of Hong Kong (No. ITS/273/16FP). The authors would like to thank the MCPF and NFF of HKUST for technical support. Helpful discussions with C. W. Tang, Y.T. Wan, and B. Shi are also acknowledged.

References:

[1] R. Yan, D. Gargas, and P. Yang, Nature Photon. 3, 569 (2009).

[2] J. C. Johnson, H. Yan, P. Yang, and R. J. Saykally, J. Phys. Chem. 107, 8816 (2003).

[3] J. X. Ding, J. A. Zapien, W. W. Chen, Y. Lifshitz, S. T. Lee, and X. M. Meng, Appl. Phys. Lett. 85, 2361 (2004).

[4] R. Agarwal, C. R. Barrelet, and C. M. Lieber, Nano Lett. 5, 917 (2005).

[5] X. Duan, Y. Huang, R. Agarwal, and C. M. Lieber, Nature. 421, 241 (2003).

[6] J. C. Johnson, H.-J. Choi, K. P. Knutsen, R. D. Schaller, P. Yang, and R. J. Saykally, Nat. Mater. 1, 106 (2002).

[7] S. Gradecak, F. Qian, Y. Li, H.-G. Park, and C. M. Lieber, Appl. Phys. Lett. 87, 173111 (2005).

[8] R. Chen, T.-T. D. Tran, K. W. Ng, W. S. Ko, L. C. Chuang, F. G. Sedgwick, and C. Chang-Hasnain, Nat. Photonics. 5, 170 (2011).

[9] D. Saxena, S. Mokkapati, P. Parkinson, N. Jiang, Q. Gao, H. H. Tan, and C. Jagadish, Nat. Photonics 7, 963 (2013).

[10] B. Mayer, L. Janker, B. Loitsch, J. Treu, T. Kostenbader, S. Lichtmannecker, T. Reichert, S. Morkötter, M. Kaniblr, G. Abstreiter,C. Gies, G. Koblmüller, and J. J. Finley, Nano Lett. 16, 152 (2016).

[11] Y. Tatebayashi, S. Kako, J. Ho, Y. Ota, S. Iwamoto, and Y. Arakawa, Nat. Photonics. 9, 501 (2015).

[12] Z. Wang, B. Tian, M. Paladugu, M. Pantouvaki, N. Le Thomas, C. Merckling, W. Guo, J. Dekoster, J. Van Campenhout, P. Absil, and D. Van Thourhout, Nano Lett. 13, 5063 (2013).

[13] Z.C Wang, B. Tian, M. Pantouvaki, W.M Guo, P. Absil, J.V. Campenhout, C. Merckling, and D. V. Thourhout, Nat. Photonics. 9(12), 837-842 (2015).

[14] Q. Gao, D. Saxena, F. Wang, L. Fu, S. Mokkapati, Y. Guo, L. Li, J. Wong- Leung, P. Caroff, H. H. Tan, and C. Jagadish, Nano Lett. 14, 5206 (2014).

[14] A. H. Chin, S. Vaddiraju, A. V. Maslov, C. Z. Ning, M. K. Sunkara, and M. Meyyappan, Appl. Phys. Lett. 88, 163115 (2006).

[16] B. Hua, J. Motohisa, Y. Kobayashi, S. Hara, and T. Fukui, Nano Lett. 9, 112 (2009).

[17] D. Lang and J. E. Bowers, Nature Photon. 4, 511 (2010).

[18] A. L. Liu, C. Zhang, J. Norman, A. Snyder, D. Lubyshev, J. M. Fastenau, A. W. K. Liu, A. C. Gossard, and J. E. Bowers, Appl. Phys. Lett. 104, 041104 (2014).

[19] S.M. Chen, W. Li, Wu. J, Q, M.C. Tang, S. Shutts, S.N. Elliott, A. Sobiesierski, A.J. Seeds, I. Ross, P.M. Smowton, and H.Y. Liu, Nat. Photonics (2016).

[20] Y. Wan, Q. Li, A. Y. Liu, A. C. Gossard, J. E. Bowers, E. L. Hu, K. M. Lau, Optics Letters 41 (7), 1664 (2016).

[21] B. Shi, S. Zhu, Q. Li, C.W Tang, Y.T. Wan, E.L. Hu, and K.M. Lau. Appl. Phys. Lett. 110, 121109 (2017).

[22] F. Schuster, J. Kapraun, G.N. Malheiros-Silveira, S. Deshpande, and C.J. Chang-Hasnain. Nano Lett.17, 2697-2702(2017).

[23] H. Kim, W.J. Lee, A.C. Farrell, J.S Morales, P.N. Senanayake, S.V. Prikhodko, T. Ochalski, and D.L. Huffaker. Nano Lett. 17 (6), 3465-3470(2017).

[24] B. Tian, Z. Wang, M. Pantouvaki, P. Absil, J. Van Campenhout, C. Merckling, and D. Van Thourhout, "Room temperature O-band DFB laser array directly grown on (001) silicon," Nano Lett. 17(1), 559–564 (2017).

[25] F.L. Lu, I. Bhattacharya, H. Sun, T.D. Tran, K.W. Ng, G.N. Malheiros-Silveira, and C.J. Chang-Hasnain. Optica. 4(7), 717-723 (2017).

[26] M. Takiguchi, A. Yokoo, K. Nozaki, M.D. Birowosuto, K. Tateno, G.Q. Zhang, E. Kuramochi, A. Shinya, and M. Notomi. APL Photonics. 2(4), 046106(2017).

[27] J. Z. Li, J. Bai, J-S. Park, B. Adekore, K. Fox, M. Carroll, A. Lochtefeld, and Z. Shellenbarger, Appl. Phys. Lett. 91, 021114 (2007).

[28] C. Merckling, N. Waldron, S. Jiang, W. Guo, N. Collaert, M. Caymax, E. Vancoille, K. Barla, A. Thean, M. Heyns, and W. Vandervorst, J. Appl. Phys. 115, 023710 (2014).

[29] R. Cipro , T. Baron , M. Martin , J. Moeyaert , S. David , V. Gorbenko , F. Bassani , Y. Bogumilowicz , J. P. Barnes , N. Rochat , V. Loup , C. Vizioz , N. Allouti , N. Chauvin , X. Y. Bao , Z. Ye , J. B. Pin , and E. Sanchez , Appl. Phys. Lett. **104**, 262103 (2014).

[30] B. Kunert, W. Guo, Y. Mols, B. Tian, Z. Wang, Y. Shi, D. Van Thourhout, M. Pantouvaki, J. Van Campenhout, R. Langer, and K. Barla, Appl. Phys. Lett. 109, 091101 (2016).

[31] Q. Li, Y. Han, X. Lu, and K.M Lau, IEEE Electron Device Lett. 37, 24-27 (2016).

[32] S. Li, and X. Zhou, and M. Li, and X. Kong, and J. Mi, and M. Wang, and W. Wang, and J. Pan, Appl. Phys. Lett. 108, 021902 (2016).

[33] Q. Li, K. W. Ng, and K. M. Lau, Appl. Phys. Lett. 106, 072105 (2015).

[34] T. Orzali, A. Vert, B. O'Brien, J. L. Herman, S. Vivekanand, S. S. Papa Rao, and S. Oktyabrsky, J. Appl. Phys. 120, 085308 (2016).

[35] Y. Han, Q. Li, S.P. Chang, W.D. Hsu, and K.M. Lau, Appl. Phys. Lett. 108, 242105 (2016).

[36] Y. Han, Q. Li, and K. M. Lau. J. Appl. Phys. 120, 245701 (2016).

[37] G. Biasiol, A. Gustafsson, K. Leifer, and E. Kapon, Phys. Rev. B 65, 205306 (2002).

[38] L. Megalini, B. Bonef, B.C. Cabinian, H.W Zhao, A. Taylor, J.S. Speck, J.E. Bowers, and J. Klamkin. Appl. Phys. Lett. 111(3), 032105, (2017).

[39] T. Stettner, P. Zimmermann, B. Loitsch, M. Doblinger, A. Regler, B. Mayer, J. Winnerl, S. Matich, H. Riedl, M. Kaniber, G. Abstreiter, G. Koblmuller, and J. J. Finley, Appl. Phys. Lett. 108, 011108 (2016).

Figure Captions

Figure 1. (a) Top-view SEM image of the as-grown highly-ordered InP/InGaAs nano-ridge array on (001) Si; (b) 70° tilted-view SEM image showing multi-faceted InP/InGaAs nano-ridge array inside V-grooved Si pockets; (c) Cross sectional SEM image of one typical InP nano-ridge with five uniform InGaAs ridge QWs.

Figure 2. (a) Cross-sectional TEM image (perpendicular to the trench direction) of one representative InP/InGaAs nano-ridge on (001) Si; (b) Zoomed in TEM image showing the generation of stacking faults at the III-V Si interface and the confinement of defects inside the V-grooved pocket; (c) Zoomed-in TEM image of the tip region of the five InGaAs ridge QWs; (d) Zoomed-in TEM image of the five InGaAs ridge QWs at one side of the InP nano-ridge. The thickness of the InGaAs QW is around 7 nm and the thickness of the InP spacer is around 28 nm; (e) TEM image along the trench direction; (f) Zoomed-in TEM image of the III-V/Si interface indicates the formation of threading dislocations and stacking faults.

Figure 3. PL spectra of the as-grown InP/InGaAs nano-ridges measured at 4.5 K and 300 K.

Figure 4. (a) Schematic of the transferred InP/InGaAs nano-ridge on a SiO_2/Si substrate; (b) Microscopic image of the transferred InP/InGaAs nano-ridge. Zoomed-in SEM image illustrates high end-facet quality; (c) PL spectra of the transferred InP/InGaAs nano-ridge under different excitation levels. Strong FP mode resonance is observed.

Figure 5. (a) Emission spectra of the InP/InGaAs nano-ridge under increasing excitation levels at 4.5 K, showing FP resonance modes at low pumping power density and stimulated emission at high pumping power density. (b) Clear threshold knee behavior in the lasing L-L curve, and sudden reduction of the line-width of lasing peak at 1410 nm as pumping level increases. (c) The blue-shift of the lasing peak at 1410 nm with increasing excitation level due to band-filling effects. (d) Cavity modes at 1410 nm and 1418 nm measured just below threshold. The line-width are 0.48 nm and 0.52 nm for peaks at 1410 nm and 1418 nm respectively. The 7.7 nm FSR agrees well with the nano-ridge length. Inset shows the electrical field distribution of the lasing transverse mode TE_{01}.

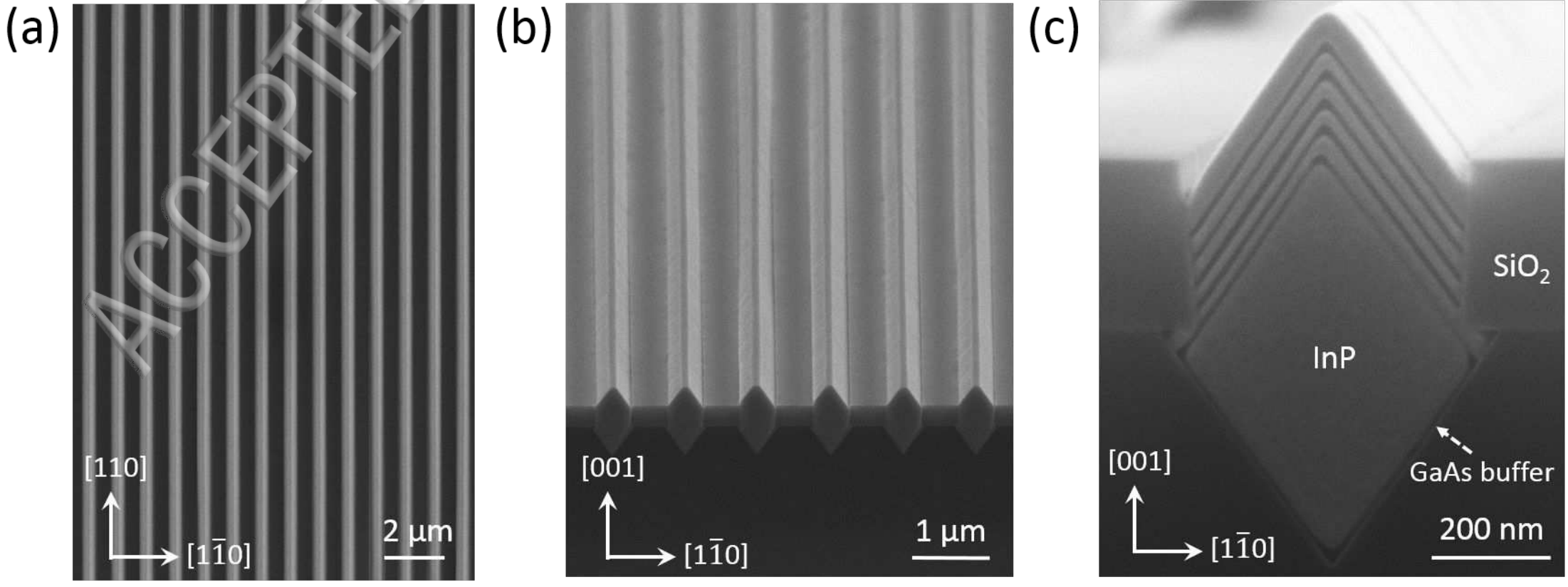
(a)
[110]
[1$\bar{1}$0]
2 µm
(b)
[001]
[1$\bar{1}$0]
1 µm
(c)
SiO_2
InP
GaAs buffer
[001]
[1$\bar{1}$0]
200 nm

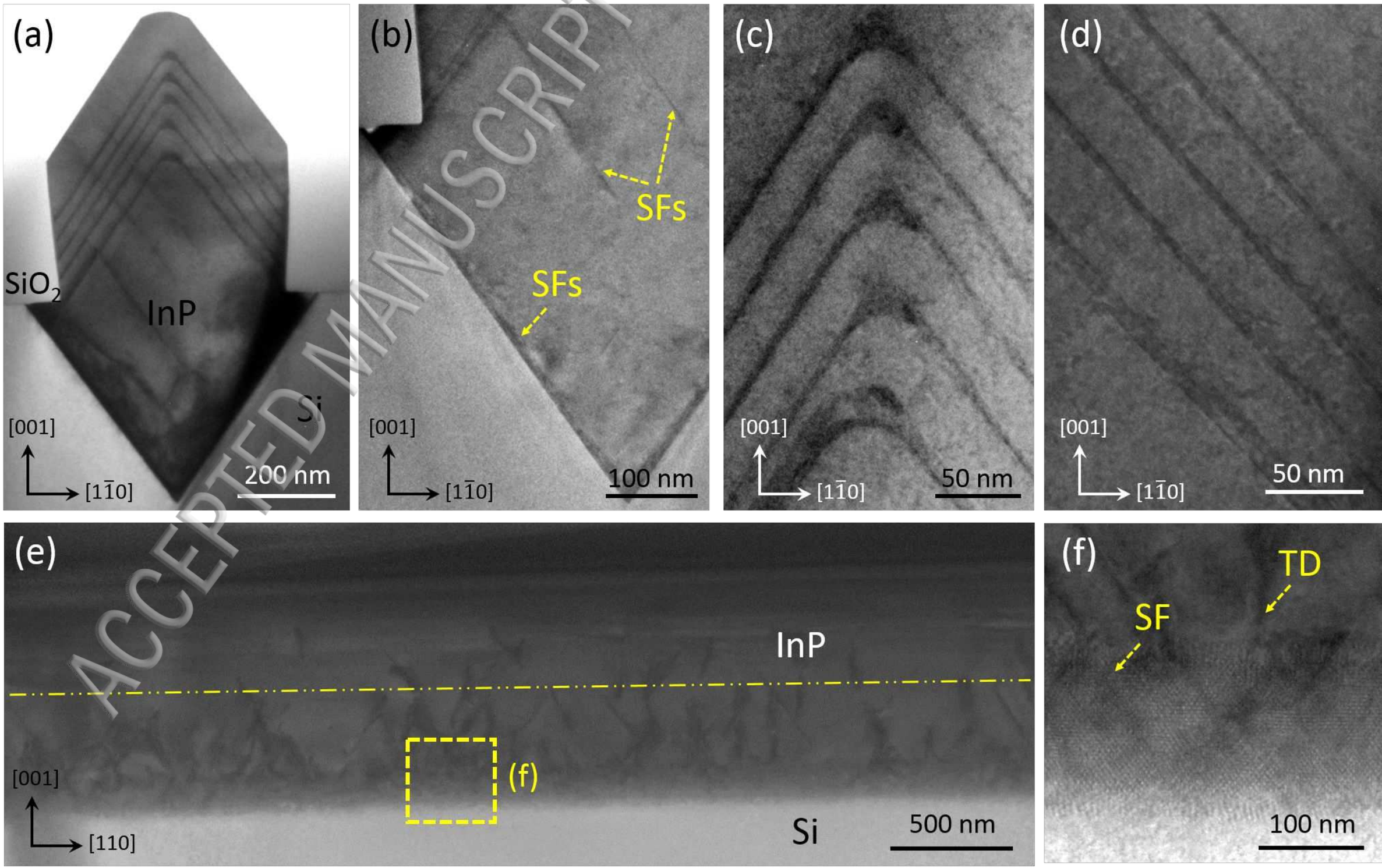

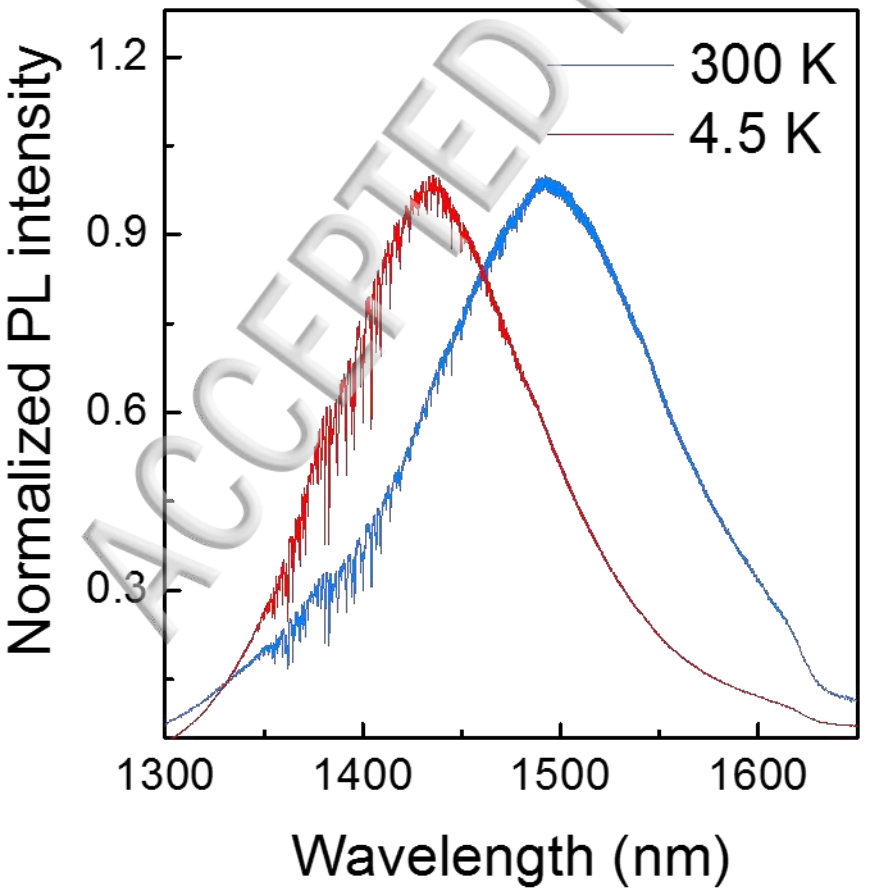
Normalized PL intensity
1.2
0.9
0.6
0.3
300 K
4.5 K
1300
1400
1500
1600
Wavelength (nm)